A Free-Standing High-Output Power Density Thermoelectric Device Based on Structure-Ordered PEDOT:PSS

Zaifang Li, Hengda Sun, Ching-Lien Hsiao, Yulong Yao, Yiqun Xiao, Maryam Shahi, Yingzhi Jin, Alex Cruce, Xianjie Liu, Youyu Jiang, Wei Meng, Fei Qin, Thomas Ederth, Simone Fabiano, Weimin Chen, Xinhui Lu, Jens Birch, Joseph W. Brill, Yinhua Zhou, Xavier Crispin and Fengling Zhang

Li, Z., Sun, H., Hsiao, C., Yao, Y., Xiao, Y., Shahi, M., Jin, Y., Cruce, A., Liu, X., Jiang, Y., Meng, W., Qin, F., Ederth, T., Fabiano, S., Chen, W., Lu, X., Birch, J., Brill, J. W., Zhou, Y., Crispin, X., Zhang, F., (2018), A Free-Standing High-Output Power Density Thermoelectric Device Based on Structure-Ordered PEDOT:PSS, *Advanced Electronic Materials*, 4(2), 1700496.
https://doi.org/10.1002/aelm.201700496

Original publication available at:
https://doi.org/10.1002/aelm.201700496

DOI: 10.1002/ (aelm.201700496)
Article type: Full Paper

A Free-standing High-output Power Density Thermoelectric Device Based on Structure-ordered PEDOT:PSS

Zaifang Li, Hengda Sun, Ching-Lien Hsiao, Yulong Yao, Yiqun Xiao, Maryam Shahi, Yingzhi Jin, Alex Cruce, Xianjie Liu, Youyu Jiang, Wei Meng, Fei Qin, Thomas Ederth, Simone Fabiano, Weimin M. Chen, Xinhui Lu, Jens Birch, Joseph W. Brill, Yinhua Zhou, Xavier Crispin*, and Fengling Zhang**

Dr. Z. F. Li, Dr. C-L. Hsiao, Y. Z. Jin, Dr. A. Cruce, Dr. X. J. Liu, Dr. T. Ederth, Prof. W. M. Chen, Prof. J. Birch, Prof. F. Zhang
Department of Physics, Chemistry and Biology (IFM)
Linköping University, SE-58183 Linköping, Sweden
E-mail: fengling.zhang@liu.se

Dr. Z. F. Li, Dr. Y. Y. Jiang, W. Meng, F. Qin, Prof. Y. H. Zhou
Wuhan National Laboratory for Optoelectronics, School of Optical and Electronic Information, Huazhong University of Science and Technology, 430074 Wuhan, China
E-mail: yh_zhou@hust.edu.cn

Dr. H. D. Sun, Dr. S. Fabiano, Prof. X. Crispin
Department of Science and Technology, Organic Electronics,
Linkoping University, SE-601 74 Norrkoping, Sweden
E-mail: xavier.crispin@liu.se

Y. L. Yao, M. Shahi, Dr. J. W. Brill
Department of Physics and Astronomy
University of Kentucky
KY 40506-0055 Lexington, USA

Y. Q. Xiao, Dr. X. H. Lu
Department of Physics, The Chinese University of Hong Kong
New Territories, Hong Kong

Prof. Y. H. Zhou
State Key Laboratory of Luminescent Materials and Devices
South China University of Technology
510640 Guangzhou, China

Dr. Z. F. Li and Dr. H. D. Sun contributed equally to this work.

Keywords: free-standing PEDOT:PSS film, p-type, thermoelectric generators, output power density

Abstract

A free-standing high-output power density polymeric thermoelectric (TE) device is realized based on a highly conductive (~2500 S/cm) structure-ordered poly (3,4-ethylenedioxythiophene):polystyrene sulfonate film (denoted as FS-PEDOT:PSS) with a Seebeck coefficient of 20.6 μV K^{-1}, an in-plane thermal conductivity of 0.64 $Wm^{-1}K^{-1}$, and a peak power factor of 107 μW $K^{-2}m^{-1}$ at room temperature. Under a small temperature gradient of 29 K, the TE device demonstrates a maximum output power density of 99 ± 18.7 μW cm^{-2}, which is the highest value achieved in pristine PEDOT:PSS based TE devices. In addition, a five-fold output power is demonstrated by series connecting 5 devices into a flexible thermoelectric module. The simplicity of assembling the films into flexible thermoelectric modules, the low out-of-plane thermal conductivity of 0.27 $Wm^{-1}K^{-1}$ and free-standing feature indicates the potential to integrate the FS-PEDOT:PSS TE modules with textiles to power wearable electronics by harvesting human body's heat. In addition to the high power factor, the high thermal stability of the FS-PEDOT:PSS films up to 250 ºC is confirmed by in-situ temperature-dependent x-ray diffraction (XRD) and grazing incident wide angle X-ray scattering (GIWAXS), which makes the FS-PEDOT:PSS films promising candidates for thermoelectric applications.

1. Introduction

Thermoelectric materials directly converting heat into electrical energy have received widespread attention nowadays due to their huge potential for applications in harvesting various wasted heat energy.[1] Recently, organic thermoelectric materials, as an emerging field, have undergone rapid development although inorganic materials such as Bi_2Te_3 still dominate commercial thermoelectric applications.[2] Among organic materials, conducting polymers are considered to be the most promising and are intensively studied. Compared to their inorganic counterparts, conducting polymers have advantages such as light-weight, non-toxicity, material abundance, easy processability, and suitability for flexible and wearable applications.[3] Furthermore, the organic materials have better biocompatibility than inorganic materials, which make them the best candidates for applications related to human body and bio-sensing.

The performance of a thermoelectric material is generally valued by the dimensionless thermoelectric figure of merit: ZT, defined as ZT = $S^2\sigma T/\kappa$, where S is the Seebeck coefficient, σ represents the electrical conductivity, and κ is the thermal conductivity. It is straightforward to have a high ZT by choosing a thermoelectric material possessing a high S and σ, but a low κ. However, the three parameters are not independent of each other, but are interrelated by carrier concentration and charge transporting mode. For instance, S as an indicator of the average entropy transported per charge carrier decreases while σ increases with carrier concentration. Since charge carriers can also transport heat, an increase in carrier concentration will also induce higher κ.[4] Therefore, the effort to optimize the performance of a thermoelectric material is always a trade-off among these three parameters. Up to now, it is still very challenging to find materials simultaneously having high σ, high S and low κ, or to efficiently increase ZT of a given material.

Among the conducting polymers, poly (3,4-ethylenedioxythiophene) (PEDOT) based materials are the most explored due to their environmental stability, aqueous solution processability, high σ of over 10^3 S/cm and low κ.[5] To enhance ZT of PEDOT, many methods are employed for improving the σ of thin PEDOT films (~100 nm).[6] For example, a high σ over 3000 S/cm has been achieved by sulfuric acid post-treatment on the films.[7] Another effective way to realize high thermoelectric performance is to increase ***S***. To reach this goal, an n-type doping strategy has been developed by X. Crispin *et al.* to tune the oxidation level and charge carrier concentration.[8] A record-high power factor of 324 μW m^{-1} K^{-2} is achieved from PEDOT-Tos materials at the oxidation level of 22% due to its very high ***S*** of 780 μV K^{-1}. Recently, the highest ZT of 0.42 is reported for thin PEDOT:PSS film by K. P. Pipe *et al.*.[9]

However, from an application point of view, not only are the thermoelectric properties of materials important, but also of concern are the output power density, thermal stability, and geometry of thermoelectric generators or modules. Nevertheless, so far, most efforts have been still devoted to improving the thermoelectric properties of various PEDOT:PSS based materials. Very few articles demonstrated PEDOT:PSS based TE devices. In 2011, O. Bubnova *et al*. fabricated the first thermoelectric module based on PEDOT-Tos and TTF-TCNQ showing a maximal output power density of 0.27 μW cm^{-2} under a temperature gradient of 30 K.[8b] D. B. Zhu et al. reported an organic TE module by incorporating p-type material poly[Cux(Cu-ett)] and n-type material poly[Nax(Ni-ett)], which demonstrated a record output density of 2.8 μW cm^{-2} for organic TE devices under a temperature bias of ΔT = 80 K.[10] Later, a high output power density of 1.75 μW cm^{-2} in a free-standing TE device based on composite system composed of PEDOT:PSS, nanofibrillated cellulose (NFC), glycerol, and dimethylsulfoxide (DMSO) was demonstrated.[11] Very recently, a record power

density of 60 μW cm^{-2} has been reported by K. Kirihara et al. with a free standing composite TE device by employing nonwoven fabric as a holder for PEDOT:PSS.[12]

From the perspective of applications, thermoelectric generators (TEGs) containing a large number of thermoelectric generating units connected in series are needed to achieve considerable power output. Hard or flexible substrates supporting thin PEDOT films in TEGs not only cause heat leakage,[11, 13] but limit the output power density from the modules because of the small ratios of PEDOT film thicknesses (~100 nm) to substrate thicknesses. Therefore, thick free-standing high conducting PEDOT:PSS films are highly desired for achieving high power density TEGs via involving less or even no supporting substrates. However, it is challenging to fabricate a free-standing PEDOT:PSS film via normal film-forming methods (such as spin-coating, printing) from a commercial PEDOT:PSS solution due to its low concentration (about 1.3%). Even though some groups succeeded in obtaining thick PEDOT:PSS films, their thermoelectric properties were limited by their moderate electrical conductivities.[14] Very recently, we developed a novel method for fabricating micro-meter thick free-standing PEDOT:PSS films (FS-PEDOT:PSS) that has a great potential for large area device processing, and has been applied in high performance supercapacitors.[15] However, the potential of FS-PEDOT:PSS in thermoelectric applications has not been explored, yet.

Here, we report on the investigation on the thermoelectric properties of these FS-PEDOT:PSS films and a free-standing high-output power density polymeric thermoelectric (TE) device based on the film. The pristine FS-PEDOT:PSS film, fabricated without using extra doping, possesses an ***S*** of 20.6 μV K^{-1} and a power factor of 107 μW $K^{-2}m^{-1}$ at room temperature. Under a small heat gradient of 29 K, the FS-PEDOT:PSS TE device exhibits an output power density of 99 μW cm^{-2}, which is the highest reported value for the same kind of PEDOT based devices. The films had moderate thermal conductivity of 0.64 $Wm^{-1}k^{-1}$ in plane and 0.27 Wm^{-}

$^{1}k^{-1}$ through plane. A thermoelectric module with five FS-PEDOT:PSS thermoelectric generating units are demonstrated which gives an output voltage of more than 2 mV (under temperature gradient of 25 K). In addition, *in-situ* temperature-dependent x-ray diffraction (XRD) and grazing incident wide angle X-ray scattering (GIWAXS) measurement prove regular arrangement of PEDOT molecules and good thermal stability of the FS-PEDOT:PSS up to 250 ºC. All the above results demonstrate its great potential for applications in low-power electronics, especially for wearable and bio-sensing electronics.

2. Results and Discussion

2.1. Thermoelectric Properties

The thermoelectric performance is investigated by fabricating a four-probe device with a structure of glass/gold electrodes/FS-PEDOT:PSS (**Figure 1a**). The conductivity and ***S*** of the FS-PEDOT:PSS film (Sample A, treated with sulfuric acid for a week) are 2500 S/cm and 20.6 μV K^{-1} at room temperature, which results in a power factor of 107 μW $K^{-2}m^{-1}$. For comparison, we fabricate thin PEDOT:PSS film (96 nm) treated by 80% sulfuric acid at 110 ℃ for 3 minutes on the same substrate. The thin film demonstrates a conductivity of 2673 S/cm, Seebeck coefficient of 15.6 μV K^{-1} and power factor of 65 $\mu Wm^{-1}K^{-2}$. The reduced Seebeck coefficient and power factor of thin films compared with FS-PEDOT:PSS should be caused by the heat leakage from the substrate, which is consistent with previous reports.[11, 13] In order to study the relationship between conductivity and Seebeck coefficient inside this FS-PEDOT:PSS, we exposed the film to tetrakis(dimethylamino)ethylene (TDAE) vapor so as to tune the oxidation level of PEDOT (referred to as “doping”). Because TDAE is a strong reducing agent, the σ value of the PEDOT:PSS film decreased from 2500 S/cm to 388 S/cm while ***S*** increases from 20 μV/K to 31 μV/K; a similar effect was observed for other PEDOT derivatives in previous studies.[8b] To compare, another sample (noted as Sample B) is prepared with a shorter treatment time of sulfuric acid for 2 hours. Sample B has lower σ

(1053 S/cm) and $\boldsymbol{S}$ (19.2 μV K^{-1}) than Sample A. Interestingly, the data of $\boldsymbol{S}$ and $\boldsymbol{\sigma}$ plotted in a graph ln $\boldsymbol{S}$ *vs.* ln $\boldsymbol{\sigma}^{-1/4}$ (**Figure 1b**) displays a linear trend but above the "universal" behavior found in many conducting polymers (dashed line).[3d] Importantly, this "universal" trend is found for conducting polymers that display temperature-activated hopping transport.[16] As previously noticed,[3d, 16] PEDOT derivatives appear above the universal behavior as we confirm here for our samples. This indicates that the transport mechanism in PEDOT might be different from pure hopping transport as suggested by the semi-metallic character identified for high Seebeck coefficient PEDOT samples.[8c] The difference between Sample A and B is interesting since it is related to the residual amount of PSS in the sample. Starting from pristine PEDOT:PSS composed of ordered PEDOT:PSS domains of high conductivity separated with disordered domains rich in PSS, we expect that the removal of PSS by sulfuric acid treatment has likely two effects: (i) to enhance the crystallinity of the ordered domains, thus promoting the formation of a bipolaron band and increasing $\boldsymbol{S}$; and (ii) to improve the connectivity of the ordered domains, thus increasing the number of percolation paths and the conductivity. Note that a similar cumulative effect of increases in Seebeck coefficient and electrical conductivity has been found when excessive PSS is removed from PEDOT:PSS by DMSO cleaning.[9]

To show the difference between the observed transport behaviors compared to the traditional hopping transport of most conducting polymers, we measure the temperature-dependent electrical conductivity in a temperature range from 200 to 400K (**Figure 1c**). It is interesting that metallic behavior (negative slope) was observed for temperatures above 325K, which is similar to the behavior of high conductivity PEDOT-Tos.[8c] Below that temperature, the FS-PEDOT:PSS demonstrates typical semiconducting behavior with a positive temperature coefficient. It implies that the FS-PEDOT:PSS possesses both semiconducting and metallic properties, as reported recently for other PEDOT derivatives.[17]

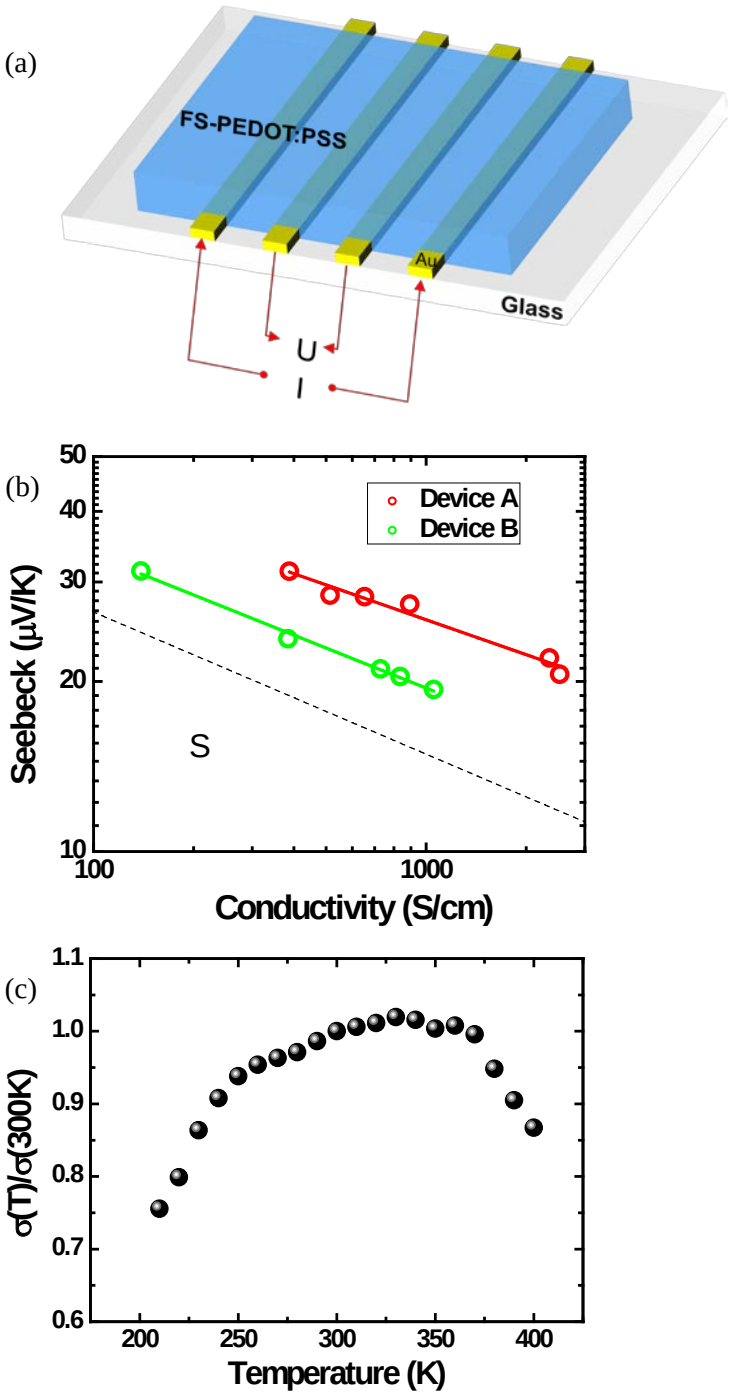

Figure 1 (a) Device structure of σ and S measurement, channel width between gold electrodes is 1 mm. (b) The relationship between σ and S of FS-PEDOT:PSS films under different doping level with TDAE, the dashed line is the indication of $S \sim \sigma^{-1/4}$. (c) Temperature dependent σ of FS-PEDOT:PSS in a temperature range from 200 to 400K.

As described in the experimental section, the in-plane (longitudinal) and through plane (transverse) thermal diffusivities were measured using ac techniques in which the sample is heated with chopped light. In short, D_{tran} = (0.17 ± 0.04) mm^2/s is determined from the frequency dependence of thermal radiation (**Figure 2a**), while D_{long} = (0.40 ± 0.08) mm^2/s is measured from the spatial dependence of the oscillating temperature when the sample is partly blocked by a movable screen (**Figure 2b**). The thermal conductivity is related to the diffusivity by $\kappa = Dc\rho$, where c = specific heat and ρ = density; assuming values of ρ = 1.37 g/cm^3 and c = 1.17 J/g·K form previous reports,[18] we find κ_{long} = (0.64 ± 0.13) $Wm^{-1}K^{-1}$ and κ_{trans} = (0.27 ± 0.06) $Wm^{-1}K^{-1}$. This value of κ_{long} is lower than ethylene glycol (EG) (κ_{long} = 0.94) and dimethyl sulfoxide (DMSO) (κ_{longs} = 1.0 $Wm^{-1}K^{-1}$) treated-PEDOT:PSS,[4, 19] presumably due to the porosity of FS-PEDOT:PSS.[15, 20] The thermal transport anisotropy $\kappa_{long}/\kappa_{trans}$ = 2.37 is lower than previously reported (3.33 for DMSO treatment and 5.6 for EG treatment).[4, 21] While the value of κ_{long} gives a modest thermoelectric coefficient of performance ZT ~ 0.05, FS-PEDOT:PSS still functions well as a TEG, as discussed below.

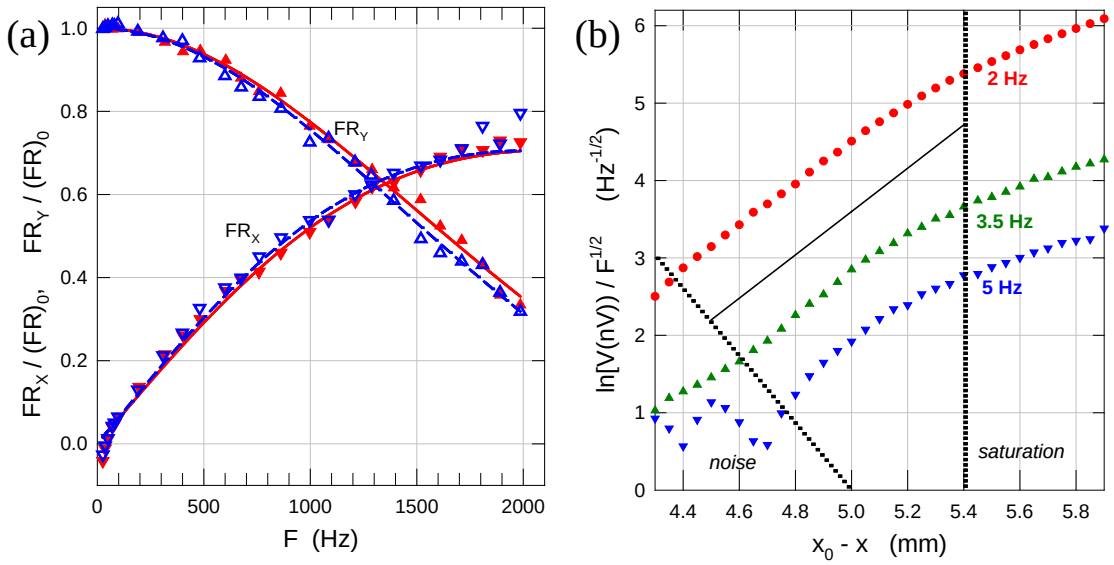

Figure 2 (a) Experimental data used to determine the through-plane diffusivity: frequency dependence of the photothermal signals in-phase (R_X) and in quadrature (R_Y) with the input

chopped light. Values are multiplied by the frequency and normalized to the values of FR at low frequency. Data is shown for two 10 μm thick samples (red and blue symbols) with the fits (lines) to Eqtn. (2). (b) Experimental data used to determine the in-plane diffusivity: spatial dependence of the thermocouple signal at a few frequencies. (x = distance between the edge of the screen and the thermocouple and x_0 = constant offset.) D_{long} is determined from the slopes between the dotted lines, as discussed in the text. A solid line with slope = 2.8/mm is shown for reference.

2.2 Free-Standing TE Device

A free-standing TE device based on FS-PEDOT:PSS film is fabricated. **Figure 3a** demonstrates the device structure while **Figure 3b** displays the output power density. The length of the device between the heat source and cold source is 1.5 cm and the width is 0.4 cm, thickness of the film is 3 μm, and the load resistance is 7 ohm, which is the same as the resistance of the film so that the output power could reach a maximum value. The output power density per cross section area of the free-standing TE device is characterized under different temperature gradients. Encouragingly, a very high output power density of 99 ± 18.7 μWcm^{-2} is achieved at a small temperature gradient of 29 K, which shows that our device possesses a much higher power density than previously reported for conducting polymers[8b, 10-11], and even higher than reported for some composite polymers (about 60 μWcm^{-2}).[12] It is worth noting that the result is achieved without optimizing the leg length of the device, and we are confident that the performance of the free-standing film can be further improved by further optimization of the device parameters. The superior output power density of the TE device can be attributed to the high conductivity of the FS-PEDOT:PSS film, the highly ordered spatial arrangement of PEDOT chains in the film and the absence of a substrate.

To demonstrate the simplicity to assemble FS-PEDOT:PSS films into practical thermoelectric applications, a prototype thermoelectric generator containing five TE devices is made (Inset

of Figure 3c). As shown in Figure 3c, the TE module demonstrates a five-fold increase of *S* (79.2 μV K^{-1}) compared to the single film (15.6 μV K^{-1}). The lower Seebeck coefficient (15.6 μV K^{-1}) might be caused by the higher PSS ratio that improves the mechanical strength of the FS-PEDOT:PSS films for fabricating free-standing thermoelectric module.

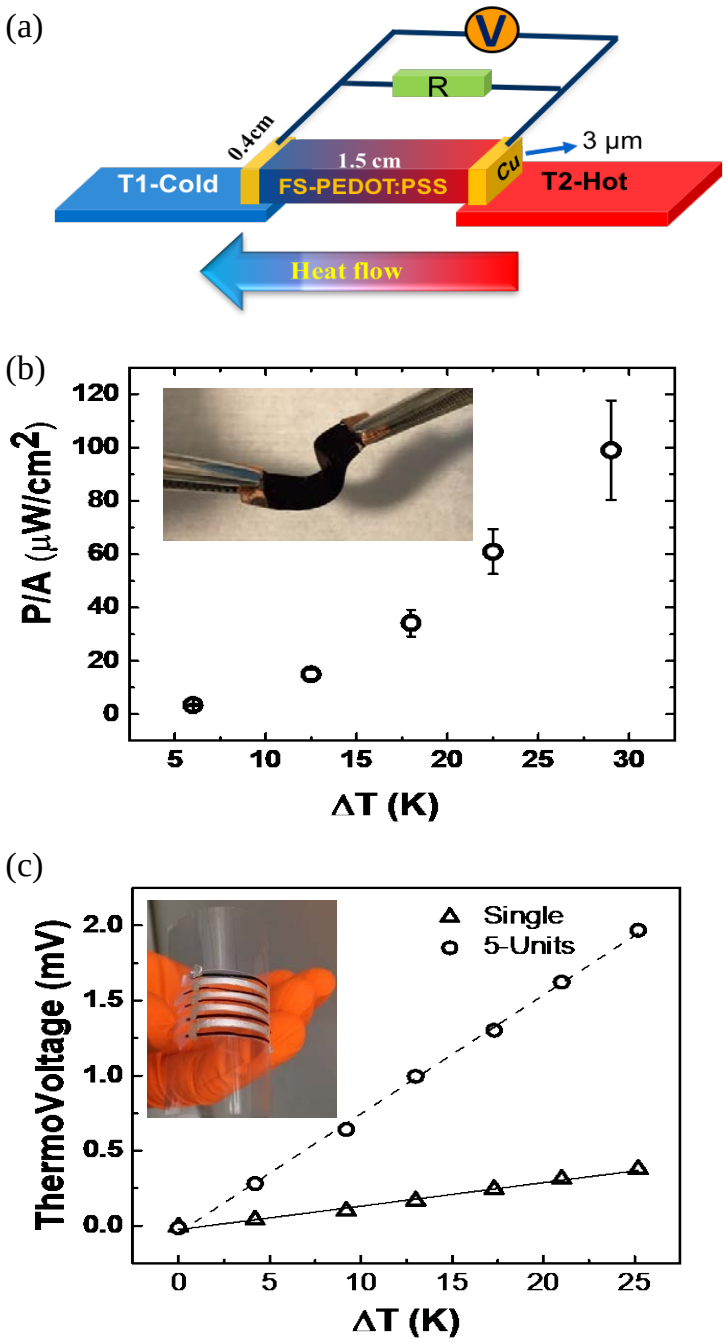

Figure 3 (a) A free standing TE device based on FS-PEDOT:PSS film. (b) Power output per cross section area of the free standing TE device. The inset is a photo-picture of the free standing TEG device. The length of the device between the heat and cold source is L=1.5 cm, film width is 0.4 cm

and the thickness of the film device is 3 μm. The load resistance is 7 ohm which is the same as the film so that the output power could reach a maximum value. (c) The voltage–temperature gradient characteristics of the FS-PEDOT:PSS based single component and module; inset is the photo-picture of the module.

2.3 Structure and Thermal Stability of the FS-PEDOT:PSS Films

To further understand the enhancement, electron paramagnetic resonance spectroscopy (EPR) is employed to detect the presence of unpaired electrons in different PEDOT:PSS films (**Figure S1**). The sulfuric acid treated FS-PEDOT:PSS film shows a weaker ESR signal than pristine PH1000 film, indicating that polaron pairs or bipolarons are the main type of charge carriers after the PEDOT:PSS film is treated with concentrated sulfuric acid.

In order to investigate the molecule spacing arrangement and thermal stability of FS-PEDOT:PSS film, temperature-dependent XRD is performed. **Figure S2a** demonstrates the XRD measurement of FS-PEDOT:PSS films before (PEDOT:PSS paste) and after (FS-PEDOT:PSS) treatment with sulfuric acid, from which we find that the arrangement of PEDOT molecules become more regular after sulfuric acid treatment, which is consistent with the conductivity enhancement. **Figure 4a** shows temperature-dependent XRD patterns of the FS-PEDOT:PSS measured from room temperature (RT) to 350 ^{o}C. The corresponding temperature-dependence of spacing of (100) plane, d, calculated by Bragg's law $2d \sin\theta = n\lambda$, and full-width at half-maximum (FWHM) of the peak are plotted in **Figure 4b**. Here θ is the diffraction angle, λ is x-ray wavelength, for Cu-Kα: 0.154 nm, and n is an integer, for first order n = 1. Obviously, the (100) plane, peak located at around 6.4^{o}, of the FS-PEDOT:PSS has almost no change when temperature increases from RT to 250 ^{o}C. With further increasing temperature, the peak shifts to higher angle and becomes weaker and broader. When the temperature exceeds 300 ^{o}C, the peak intensity drops significantly to less than half of the RT one. After *in-situ* annealing at 350 ^{o}C in vacuum, the peak, measured at RT, shifts to ~ 10.1^{o}

and intensity drops to 1/10 of the as-grown sample. As can be seen in Figure 4b, the spacing shrinks from 1.38 nm to ~ 0.875 nm and FWHM raises from 2 to 4 degree. The dynamics of structural degradation is further studied by isothermal-heat-treatment XRD measurement at 100 °C, 300 °C, and 350 °C, kept for 1 hour. **Figure S2b** shows that the structure degrades dynamically when the PEDOT:PSS starts to decompose at high temperature, 300 °C, and 350 °C. The decomposition process terminates when the sample is cooled down to RT. It seems that the structure is permanently damaged after annealing. The shrinkage of the lattice is probably due to the loss of material while the periodic stacking of the fibers remains. The above results show that the FS-PEDOT:PSS film exhibits excellent thermal stability in chemical as well as crystalline structure for temperatures < 250 °C.

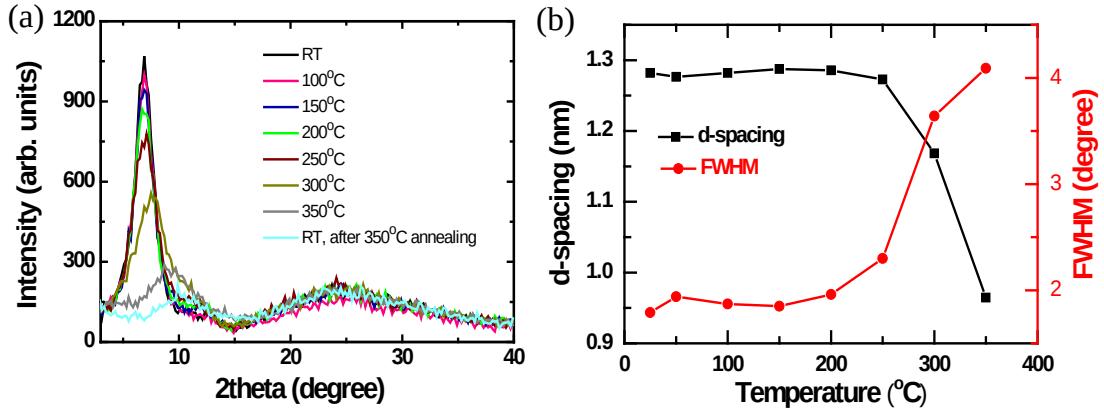

Figure 4 (a) Temperature-dependent XRD characteristics of FS-PEDOT:PSS at different temperature (room temperature (RT) to 350°C). (b) The statistics of temperature-dependent spacing (d-spacing) and full-width at half-maximum (FWHM).

XPS characteristics are carried out to further explore the composition changes of FS-PEDOT:PSS film under heating conditions (**Figure S3**). Three FS-PEDOT:PSS samples are treated at room temperature, 250 and 300 °C respectively for ten minutes in a glove box. It can be seen that the intensity around 168 eV originating from PSS decreases substantially after the FS-PEDOT:PSS samples were heated. This is mainly caused by the decomposition of PSS,

because the sulfonic acid group in PSS is not stable and SO_3 gas is generated when heated above 250 °C.[22] This result also provides a strong support for understanding the decreased molecule distance between PEDOT. Furthermore, the reduction of PSS concentration is not only helpful for the film's electrical conductivity, but also thermal and air stability, in view of its strong acidity.

To further investigate the temperature-dependent molecule packing and thermal stability of FS-PEDOT:PSS film, *in-situ* annealing grazing incident wide angle X-ray scattering (GIWAXS) measurements are also performed.[23] The two-dimensional GIWAXS patterns are presented in **Figure 5a-f**. **Figure 5g-h** present the intensity profiles for the film annealed from room temperature (RT) to 250 °C along the out-of-plane (q_z) and in-plane (q_r) directions. At RT, we observe the (100), (200), (300) and (400) peaks in the out-of-plane direction at q_z = 0.455, 0.910, 1.37 and 1.81 $Å^{-1}$ (d = 13.8 Å) and the (010) peak at q_r= 1.85 $Å^{-1}$ (d = 3.39 Å), corresponding to the lamella stacking distance of alternating PEDOT and PSS and the $\pi - \pi$ stacking of PEDOT, respectively.[24] This is in good agreement with the XRD results as the (100) peak located at around 6.4° and also indicates that the FS-PEDOT:PSS film has high crystallinity and aligns in preferred orientation with respect to the substrate. As the temperature is gradually increased to 250 °C, the FS-PEDOT:PSS film maintained the similar scattering pattern, providing further evidence to the remarkable thermal stability and therefore the observed high conductivity.

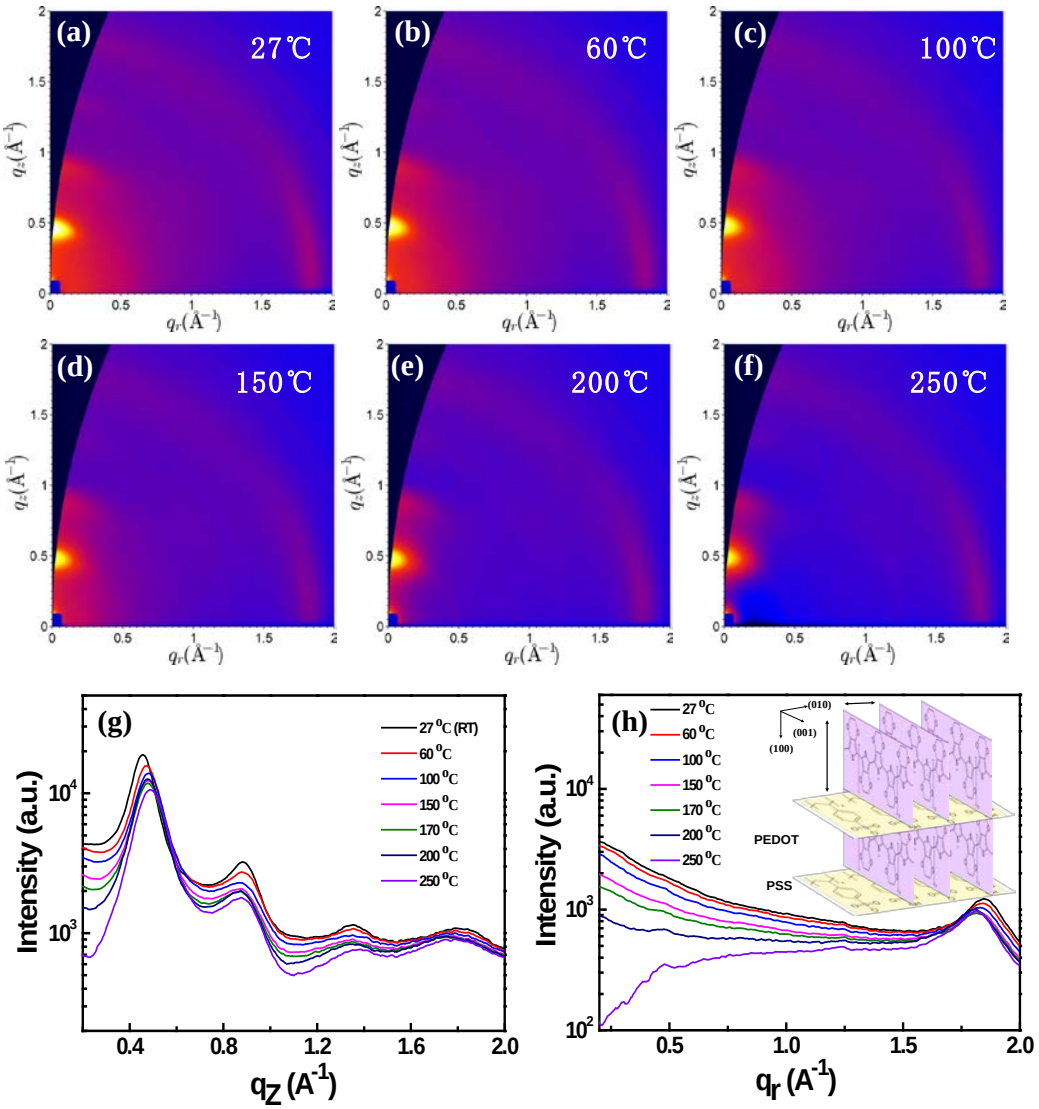

Figure 5 2D GIWAXS patterns of the FS-PEDOT:PSS film (a) without annealing and (b-f) in-situ annealed with increasing temperatures. GIWAXS intensity profiles along the (g) out-of-plane and (h) in-plane (Inset: Illustration of crystalline FS-PEDOT:PSS) directions.

3. Conclusion

A high power factor (107 μW K^{-2}m^{-1}) has been demonstrated with free-standing conducting polymer PEDOT:PSS films, with an output power density of 99 ± 18.7 μW cm^{-2} in a corresponding free-standing TE device under a temperature gradient of 29 K. The high thermoelectric performance of the TE device is attributed to the high conductivity of the thick PEDOT:PSS films, derived from the ordered stacking structure of the PEDOT chains and the

absence of a substrate. The ordered structure is stable up to 250 ^{o}C. The results indicate that FS-PEDOT:PSS thermoelectric devices have huge potential for applications in low-power electronics in the future. One more advantage of the FS-PEDOT:PSS films over their thin PEDOT:PSS counterparts is the possibility to be used in a vertical geometry embedded in a textile to harvest heat from human body for powering wearable electronics.

4. Experimental Section

Preparation of FS-PEDOT:PSS: The detailed preparation procedure of the FS-PEDOT:PSS film is similar to that of our previous report.[15] The critical point of this strategy is to increase the PEDOT:PSS particle size assisted by diluted 1M H_2SO_4, which is confirmed by a Dynamic Light Scattering (DLS) measurement (**Figure S4**). A high concentration H_2SO_4 (99.99%) is employed to treat the FS-PEDOT:PSS film for a week to achieve high conductivity of 2500 S/cm.[7] **Figure S5** presents the Scanning electron microscope (SEM) photographs of the surface (a, c) and cross-section (b, d) of free standing PEDOT:PSS films before and after treated by concentrated sulfuric acid, from which we can find that the treated film demonstrates a layer by layer structure. This morphology is consistent with the improved conductivity.

Conductivity and thermoelectric characterization of FS-PEDOT:PSS: As for the conductivity measurement, we use a four-probe approach to measure the *I-V* of the film and thereby calculate out the conductivity. We firstly fabricate the glass substrate with four evaporated gold electrodes with thickness of 20 nm, width of 1 mm, length of 1.5 cm and channel length of 1 mm. The gold electrodes are fabricated by vacuum deposition with a thin adherent layer of Cr between gold and glass. Then FS-PEDOT:PSS film is directly paved onto this glass substrate under wetting condition with the help of a nitrogen gas gun. The current-voltage (*I-V*) characteristic is measured by a Keithley 4200. The film thickness is measured by step profiler of DEKTAK 150. Then the conductivity is calculated from the following equation:

$$\sigma = IL/VA \qquad (1)$$

Here, σ is conductivity, *I* is the current, L is the channel length, *V* is the voltage, A is the cross area of the sample.

For the ***S*** measurements, the samples are fixed in between a pair of Peltier modules to maintain the desired temperature difference. Here, ΔT is measured by means of thermocouples and the thermal voltage is read directly from a nanovoltmeter. Doping of FS-PEDOT:PSS is done in the glovebox by exposing the film over a bottle of TDAE so the vapor could reach the film. The doping level is tuned by changing the exposure time. After doping, the sample is sequentially measured also in the glovebox.

Thermal conductivity measurement: The transverse, through-plane thermal diffusivity, D_{trans}, is measured on two d = 10 μm pieces (area ~ 7 mm^2) of sample using an ac-photothermal technique.[25] The sample, in vacuum, is placed several mm from an infrared detector while the opposite face of the sample is illuminated with white light chopped at frequency F = ω/2π. The frequency dependence of the oscillating temperature on the back face of the sample (facing the detector) is given by:[25]

$$T_{ac} = A_0 \chi / \{\omega[\sinh\chi \cos\chi (1-i) + \cosh\chi \sin\chi (1+i)]\} \qquad (2)$$

A_0 is a constant and $\chi \equiv (90^{1/2} \omega\tau_{int}/2)^{1/2}$, where $\tau_{int} = d^2/(90^{1/2} D_{trans})$ is the internal thermal time constant of the sample,[26] and the phase is measured with respect to the incident light. For the fairly opaque samples, with a 10 μm long-wave pass filter placed the sample and detector, negligible light from the source reaches the detector. Therefore, unlike in Reference[25] we are able to fit the frequency dependence of the detector signal in-phase (R_X) as well as in quadrature (R_Y) with the incoming light, as shown in Figure 2a, where results for two samples are shown. The fitted time constants for the samples are τ_{int} = (61 ± 2) μs and (64 ± 2) μs, so with the thickness d = (10 ± 1) μm, we find D_{trans} = (0.17 ± 0.04) mm^2/s.

For the longitudinal in-plane diffusivity, D_{long}, we use the technique of Hatta, et al;.[27] A ~ 1 cm long strip of d = 10 μm material is suspended, in vacuum, on 12 μm chromel-constantan thermocouple wires which are glued to the bottom center of the sample. The top face of the strip is illuminated by white light chopped at frequency $F << 1/\tau_{int}$. A movable screen blocked most of the sample, including the part above the thermocouple. As the screen is moved a distance x, the oscillating temperature, measured by the thermocouple, is given by:[27]

$$F^{-1/2}\, d\ln T_{ac}/dx = -(\pi/D_{long})^{1/2} \qquad (3)$$

Results at three frequencies are shown in Figure 2b. The average slope, taken between the region in which the signal saturates (small x) and the region in which the signal gets lost in the noise (large x) is (2.8 ± 0.3)/mm, giving D_{long} = (0.40 ± 0.08) mm^2/s.

Fabrication of thermoelectric device and module: A free standing thermal electric device is made by cutting a 3 μm thick FS-PEDOT:PSS film into shape, and then copper paste is used for electrical connection to electrodes. Note that the copper paste is on both sides of the film, so when the sample is put on Peltier modules there was no temperature difference in the vertical (through plane) direction and the voltage is only contributed by in-plane thermal Seebeck effect. To fabricate the thermoelectric module, five rectangular openings (0.2 × 2 cm^2) are made on the PES substrates, with silver paste used between the openings as electrodes of the module. Then the FS-PEDOT:PSS film is put on the openings by fixing two ends on the PES substrate. Finally, the electrodes and FS-PEDOT:PSS films are connected in series by silver paste.

XRD and GIWAXS characterization: An *in situ* annealing XRD measurement is performed using a Philips X'Pert MPD Bragg-Brentano diffractometer equipped with a Edmund-Bühler HDK 2.4 high-temperature high-vacuum chamber with a Be window.[28] The grazing incidence wide angle X-ray scattering measurements (GIWAXS) are carried out at BL23A1

of National Synchrotron Radiation Research Center, Hsinchu. The energy of the X-ray source is set to 10 keV (wavelength of 1.24 Å) and the incident angle was 0.15°.

Supporting Information
Supporting Information is available from the Wiley Online Library or from the author.

Acknowledgements
The work is supported by Vinnova Marie Curie incoming project [2016-04112 to Z.L.], the Swedish Government Strategic Research Area in Materials Science on Functional Materials at Linköping University [200900971 to F.Z.], the Recruitment Program of Global Youth Experts [2014 to Y.Z.], the National Natural Science Foundation of China [21474035 to Y.Z.], United States National Science Foundation [DMR-1262261 to J.B.], the Open Fund of the State Key Laboratory of Luminescent Materials and Devices [2016-skllmd-03 to Y.Z.], European Research Council [ERC 307596 to X.C.]. We are grateful to Prof. Wei Xu at Chinese Academy of Sciences for preliminary characterization of the film and discussion. Y.X and X.L. the beam time and technical supports provided by 23A SWAXS beamline at NSRRC, Hsinchu. We thank Ruoyun Zhang, a visiting undergraduate student from Tsinghua University, China for helping with module template preparation.

Received: ((will be filled in by the editorial staff))
Revised: ((will be filled in by the editorial staff))
Published online: ((will be filled in by the editorial staff))

References

[1] a) L. E. Bell, *Science* **2008**, *321*, 1457; b) A. Minnich, M. Dresselhaus, Z. Ren, G. Chen, *Energy Environ. Sci.* **2009**, *2*, 466; c) Z. Fan, P. Li, D. Du, J. Ouyang, *Adv. Energy Mater.* **2017**, *7*, 1602116; d) D. Huang, C. Wang, Y. Zou, X. Shen, Y. Zang, H. Shen, X. Gao, Y. Yi, W. Xu, C.-a. Di, D. Zhu, *Angew. Chem., Int. Ed.* **2016**, *55*, 10672.

[2] a) R. Venkatasubramanian, E. Siivola, T. Colpitts, B. O'quinn, *Nature* **2001**, *413*, 597; b) X. Yan, B. Poudel, Y. Ma, W. Liu, G. Joshi, H. Wang, Y. Lan, D. Wang, G. Chen, Z. Ren, *Nano Lett.* **2010**, *10*, 3373.

[3] a) M. He, F. Qiu, Z. Lin, *Energy Environ. Sci.* **2013**, *6*, 1352; b) Q. Zhang, Y. Sun, W. Xu, D. Zhu, *Adv. Mater.* **2014**, *26*, 6829; c) Q. Zhang, Y. Sun, W. Xu, D. Zhu,

Macromolecules **2014**, *47*, 609; d) B. Russ, A. Glaudell, J. J. Urban, M. L. Chabinyc, R. A. Segalman, *Nat. Rev. Mater.* **2016**, *1*, 16050.

[4] J. Liu, X. Wang, D. Li, N. E. Coates, R. A. Segalman, D. G. Cahill, *Macromolecules* **2015**, *48*, 585.

[5] a) J. Luo, D. Billep, T. Waechtler, T. Otto, M. Toader, O. Gordan, E. Sheremet, J. Martin, M. Hietschold, D. R. Zahn, *J. Mater. Chem. A* **2013**, *1*, 7576; b) O. Bubnova, M. Berggren, X. Crispin, *J. Am. Chem. Soc.* **2012**, *134*, 16456; c) D. A. Mengistie, C.-H. Chen, K. M. Boopathi, F. W. Pranoto, L.-J. Li, C.-W. Chu, *ACS Appl. Mater. Interfaces* **2014**, *7*, 94; d) Y. H. Kim, C. Sachse, M. L. Machala, C. May, L. Müller‐Meskamp, K. Leo, *Adv. Funct. Mater.* **2011**, *21*, 1076; e) A. Weathers, Z. U. Khan, R. Brooke, D. Evans, M. T. Pettes, J. W. Andreasen, X. Crispin, L. Shi, *Adv. Mater.* **2015**, *27*, 2101; f) C. M. Palumbiny, F. Liu, T. P. Russell, A. Hexemer, C. Wang, P. Müller‐Buschbaum, *Adv. Mater.* **2015**, *27*, 3391.

[6] a) H. J. Lee, G. Anoop, H. J. Lee, C. Kim, J.-W. Park, J. Choi, H. Kim, Y.-J. Kim, E. Lee, S.-G. Lee, *Energy & Environmental Science* **2016**, *9*, 2806; b) C. Cho, K. L. Wallace, P. Tzeng, J. H. Hsu, C. Yu, J. C. Grunlan, *Adv. Energy Mater.* **2016**, *6*, 1502168; c) K. Zhang, S. Wang, X. Zhang, Y. Zhang, Y. Cui, J. Qiu, *Nano Energy* **2015**, *13*, 327; d) I. Petsagkourakis, E. Pavlopoulou, G. Portale, B. A. Kuropatwa, S. Dilhaire, G. Fleury, G. Hadziioannou, *Sci. Rep.* **2016**, *6*, 30501; e) Z. Fan, P. Li, D. Du, J. Ouyang, *Adv. Energy Mater.* **2017**, *7*, 1602116.

[7] a) Y. Xia, K. Sun, J. Ouyang, *Adv. Mater.* **2012**, *24*, 2436; b) E. J. Bae, Y. H. Kang, K.-S. Jang, S. Y. Cho, *Sci. Rep.* **2015**, *6*, 18805.

[8] a) S. Fabiano, S. Braun, X. Liu, E. Weverberghs, P. Gerbaux, M. Fahlman, M. Berggren, X. Crispin, *Adv. Mater.* **2014**, *26*, 6000; b) O. Bubnova, Z. U. Khan, A. Malti, S. Braun, M. Fahlman, M. Berggren, X. Crispin, *Nat. Mater.* **2011**, *10*, 429; c)

O. Bubnova, Z. U. Khan, H. Wang, S. Braun, D. R. Evans, M. Fabretto, P. Hojati-Talemi, D. Dagnelund, J.-B. Arlin, Y. H. Geerts, *Nat. Mater.* **2014**, *13*, 190.

[9] G.-H. Kim, L. Shao, K. Zhang, K. P. Pipe, *Nat. Mater.* **2013**, *12*, 719.

[10] Y. Sun, P. Sheng, C. Di, F. Jiao, W. Xu, D. Qiu, D. Zhu, *Adv. Mater.* **2012**, *24*, 932.

[11] A. Malti, J. Edberg, H. Granberg, Z. U. Khan, J. W. Andreasen, X. Liu, D. Zhao, H. Zhang, Y. Yao, J. W. Brill, *Adv. Sci.* **2016**, *3*, 1500305.

[12] K. Kirihara, Q. Wei, M. Mukaida, T. Ishida, *Synth. Met.* **2017**, *225*, 41.

[13] R. R. Søndergaard, M. Hösel, N. Espinosa, M. Jørgensen, F. C. Krebs, *Energy Sci. Eng.* **2013**, *1*, 81.

[14] a) J. Choi, J. Y. Lee, S. S. Lee, C. R. Park, H. Kim, *Adv. Energy Mater.* **2016**, *6*, 1502181; b) C. Liu, B. Lu, J. Yan, J. Xu, R. Yue, Z. Zhu, S. Zhou, X. Hu, Z. Zhang, P. Chen, *Synth. Met.* **2010**, *160*, 2481; c) Q. Jiang, C. Liu, H. Song, J. Xu, D. Mo, H. Shi, Z. Wang, F. Jiang, B. Lu, Z. Zhu, *Int. J. Electrochem. Sci.* **2014**, *9*, 7540.

[15] Z. Li, G. Ma, R. Ge, F. Qin, X. Dong, W. Meng, T. Liu, J. Tong, F. Jiang, Y. Zhou, *Angewandte Chemie* **2016**, *128*, 991.

[16] S. D. Kang, G. J. Snyder, *Nat. Mater.* **2017**, *16*, 252.

[17] M. N. Gueye, A. Carella, N. Massonnet, E. Yvenou, S. Brenet, J. r. m. Faure-Vincent, S. Pouget, F. Rieutord, H. Okuno, A. Benayad, *Chem. Mater.* **2016**, *28*, 3462.

[18] H. Park, S. H. Lee, F. S. Kim, H. H. Choi, I. W. Cheong, J. H. Kim, *J. Mater. Chem. A* **2014**, *2*, 6532.

[19] Q. Wei, C. Uehara, M. Mukaida, K. Kirihara, T. Ishida, *AIP Adv.* **2016**, *6*, 045315.

[20] a) J. K. Carson, S. J. Lovatt, D. J. Tanner, A. C. Cleland, *Int. J. Heat Mass Transfer* **2005**, *48*, 2150; b) R. H. Tarkhanyan, D. G. Niarchos, *APL Mater.* **2014**, *2*, 076107.

[21] Q. Wei, M. Mukaida, K. Kirihara, T. Ishida, *ACS Macro Lett.* **2014**, *3*, 948.

[22] G. Greczynski, T. Kugler, W. Salaneck, *Thin Solid Films* **1999**, *354*, 129.

[23] J. Mai, T.-K. Lau, J. Li, S.-H. Peng, C.-S. Hsu, U. S. Jeng, J. Zeng, N. Zhao, X. Xiao, X. Lu, *Chemistry of Materials* **2016**, *28*, 6186.

[24] N. Kim, S. Kee, S. H. Lee, B. H. Lee, Y. H. Kahng, Y. R. Jo, B. J. Kim, K. Lee, *Adv. Mater.* **2014**, *26*, 2268.

[25] J. Brill, M. Shahi, M. M. Payne, J. Edberg, Y. Yao, X. Crispin, J. Anthony, *J. Appl. Phys.* **2015**, *118*, 235501.

[26] P. F. Sullivan, G. Seidel, *Phys. Rev.* **1968**, *173*, 679.

[27] a) I. Hatta, Y. Sasuga, R. Kato, A. Maesono, *Rev. Sci. Instrum.* **1985**, *56*, 1643; b) H. Zhang, Y. Yao, M. M. Payne, J. E. Anthony, J. W. Brill, *Appl. Phys. Lett.* **2014**, *105*, 073302.

[28] S. Olsson, F. Eriksson, J. Birch, L. Hultman, *Thin Solid Films* **2012**, *526*, 74.

A free-standing thermoelectric (TE) device is realized based on a high conductivity (2500 S/cm) structure-ordered PEDOT:PSS film with an output power density of 99 ± 18.7 μW cm^{-2} under a gradient of 29 K, which is the highest value for pure PEDOT:PSS based TE device. Free-standing TE device presented here suggests its great potential application in low consumption wearable electronics.

Keyword: free-standing PEDOT:PSS film, p-type, thermoelectric generators, output power density

Z. F. Li, H. D. Sun, C-L. Hsiao, Y. L. Yao, Y. Q. Xiao, M. Shahi, Y. Z. Jin, A. Cruce, X. J. Liu, Y. Y. Jiang, W. Meng, F. Qin, T. Ederth, S. Fabiano, W. M. Chen, X. H. Lu, J. Birch, J. W. Brill, Y. H. Zhou*, X. Crispin*, and F. Zhang*

A Free-standing High-output Power Density Thermoelectric Device Based on Structure-ordered PEDOT:PSS

ToC figure

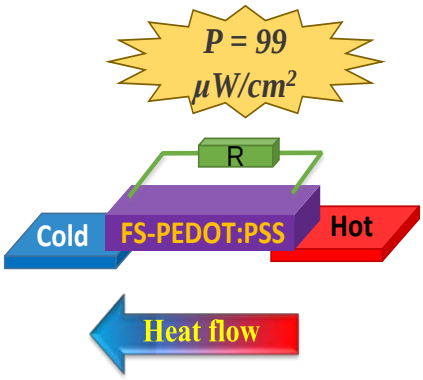

Supporting information

A Free-standing High-output Power Density Thermoelectric Device Based on Structure-ordered PEDOT:PSS

Zaifang Li, Hengda Sun, Ching-Lien Hsiao, Yulong Yao, Yiqun Xiao, Maryam Shahi, Yingzhi Jin, Alex Cruce, Xianjie Liu, Youyu Jiang, Wei Meng, Fei Qin, Thomas Ederth, Simone Fabiano, Weimin M. Chen, Xinhui Lu, Jens Birch, Joseph W. Brill, Yinhua Zhou, Xavier Crispin*, and Fengling Zhang**

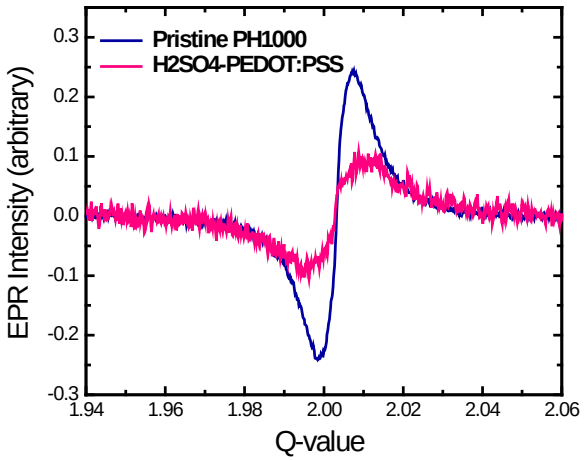

Figure S1 EPR spectra of pristine PEDOT:PSS film and concentrated sulfuric acid treated PEDOT:PSS film. The films were fabricated by spincoating method on thin-glass substrate. As for the H2SO4-PEDOT:PSS film, it was spincoated from the PEDOT:PSS paste and then treated by concentrated sulfuric acid for 10 min at room temperature.

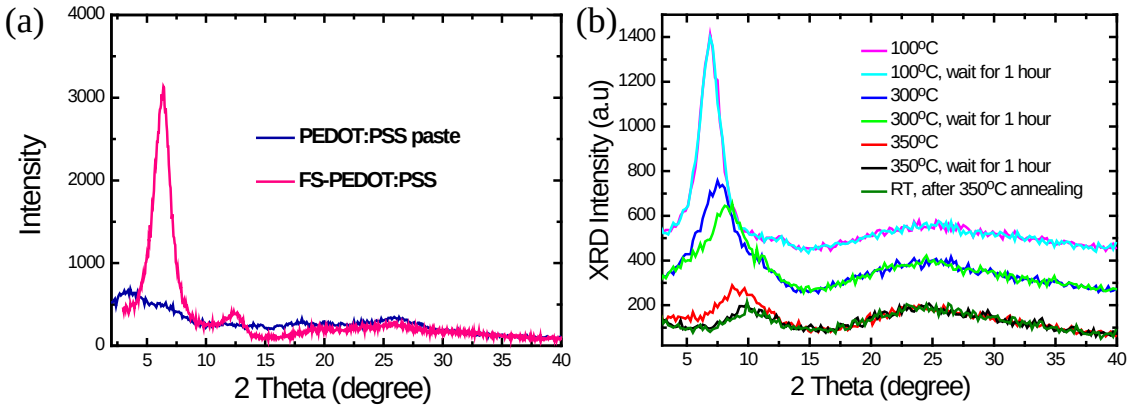

Figure S2 (a) XRD measurement of free standing PEDOT:PSS films before (PEDOT:PSS paste) and after (FS-PEDOT:PSS) concentrated sulfuric acid treated. (b)Time-dependent XRD of FS-PEDOT:PSS film at different temperatures of 100, 300 and 350°C.

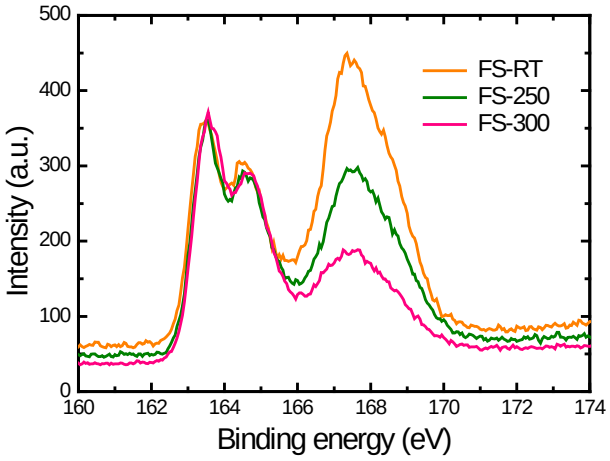

Figure S3 XPS characterization of FS-PEDOT:PSS samples treated for 10 minutes in glove box at room temperature, 250 and 300°C, repectively.

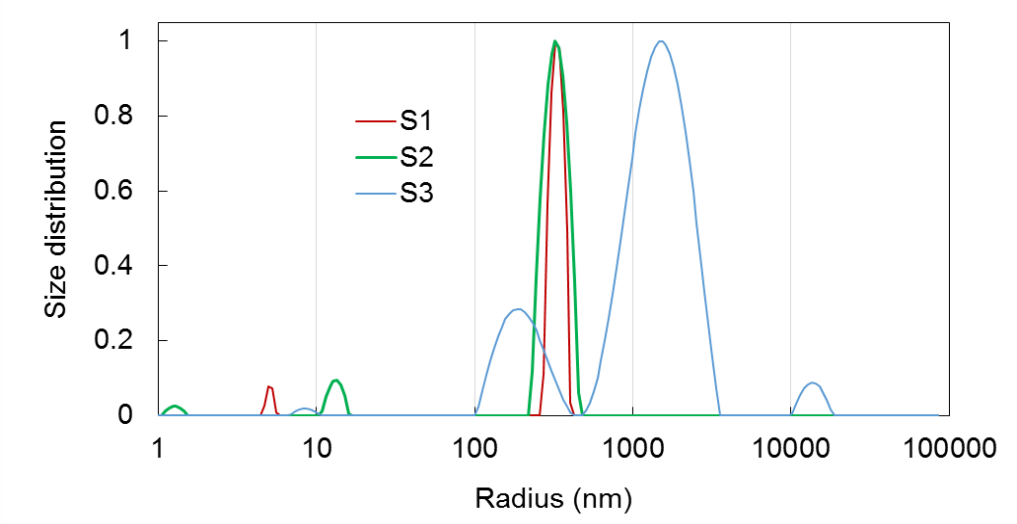

Figure S4 DLS measurement of pristine PH1000 (S1), PH1000 + 5% EG (S2) and PEDOT:PSS paste (S3).

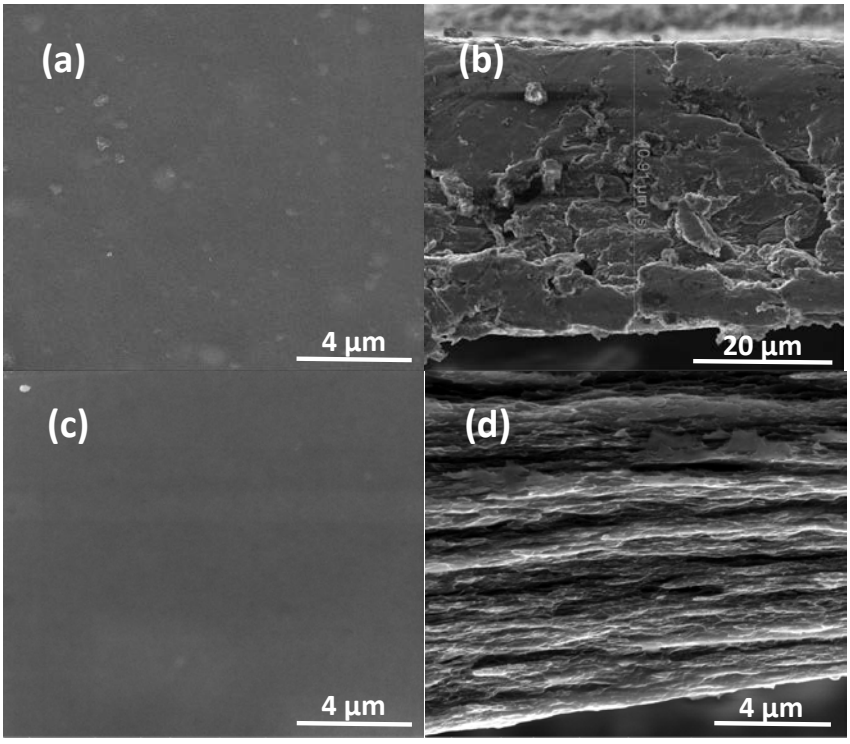

Figure S5 SEM photographs of surface (a, c) and cross-section (b, d) of free standing PEDOT:PSS films before and after treated with concentrated sulfuric acid.